


Spin dynamics in ensembles of ultrafine ferrihydrite nanoparticles

Yu. V. Knyazev ^{1,*} D. A. Balaev,^{1,2} S. A. Skorobogatov,^{1,2} D. A. Velikanov,¹ O. A. Bayukov,¹
S. V. Stolyar,^{1,2} R. N. Yaroslavtsev,¹ and R. S. Iskhakov¹

¹*Kirensky Institute of Physics, Federal Research Center KSC SB RAS, Akademgorodok 50, bld. 38, Krasnoyarsk 660036, Russia*

²*Siberian Federal University, Svobodnyy 79, Krasnoyarsk 660041, Russia*



(Received 10 January 2023; revised 7 February 2023; accepted 7 March 2023; published 14 March 2023)

Features of the spin dynamics in ensembles of interacting (FH-chem) and weakly interacting (FH-coated) magnetic ultrasmall ($d \sim 2$ nm) ferrihydrite nanoparticles have been explored. The dc and ac magnetic susceptibilities [$\chi'(T)$ and $\chi''(T)$] of the investigated samples have been thoroughly measured in a weak magnetic field (2 Oe) around the temperatures of superparamagnetic blocking of the nanoparticle magnetic moments (19 and 50.4 K for FH-coated and FH-chem, respectively, according to the dc magnetization data). It has been shown that the magnetic interactions between nanoparticles induce the formation of the cluster spin-glass state below the superparamagnetic blocking temperature ($T_g = 18$ and 49.5 K for FH-coated and FH-chem, respectively). It has been found that coating of nanoparticles increases the critical scaling index from $z\nu = 5.9$ (FH-chem) to $z\nu = 8.0$ (FH-coated). This indicates a general slowdown of the dynamics of correlated spins, which is also expressed as an increase in relaxation time τ_0 after switching on the interparticle interactions. We attribute this phenomenon to a consequence of a change in the volume of correlated spins with the increasing size of a cluster of interacting nanoparticles. It has been demonstrated using the simulated $\chi''(T)$ dependence that the dissipation of the magnetic energy occurs in two independent stages. The first stage is directly related to the blocking of the nanoparticle magnetic moments, while the second stage reflects the spin-glass behavior of surface spins and depends strongly on the intensity of the interparticle interactions.

DOI: [10.1103/PhysRevB.107.115413](https://doi.org/10.1103/PhysRevB.107.115413)

I. INTRODUCTION

The temperature behavior of the nonergodic magnetic systems depends strongly on the initial conditions [1,2], since such systems can be in a great number of different states with the low energy close to the energy of the ground state, even in the low-temperature limit [3]. Examples of the nonergodic magnetic systems are both highly diluted and concentrated alloys of magnetic metals [4,5] and magnetic dielectrics with the strongly frustrated magnetic interactions [6,7], in which the spin-glass state is established. The real part of the ac magnetic susceptibility of these materials has a peak and its imaginary part increases sharply around the magnetic transition. However, the temperature dependence of the heat capacity often contains no singularities that would be indicative of the occurrence of phase transitions [8]. Therefore, both theoretical and experimental studies of such systems seem to be a nontrivial task.

According to the theory, in the magnetically ordered structural region of the discussed materials, weakly interacting areas (droplets) of bound spins surrounded by an energy wall are formed. The droplets should have the minimum energy. This representation of spin glasses is called the droplet model [9]. Within the droplet model, a single spin-glass domain can be considered as a droplet or a cluster with the volume changing in time or with a decrease in temperature due

to the nonequilibrium spin dynamics [10]. The droplet size is determined by the correlation length, which is an important characteristic of such systems and can attain tens of nanometers. A record correlation length of ~ 150 nm has recently been reported for a single-crystal CuMn (6 at. %) sample [11,12].

Such scales of the interaction between the magnetic moments in bulk materials are comparable with nanoparticle sizes in powder systems and can therefore be implemented not only in bulk spin glass. An obvious analog is ensembles of single-domain nanoparticles, in which the volume of interacting spins is physically limited by a nanoparticle size. It is known well that nanoparticle ensembles can behave as bulk spin glass [13,14]. This behavior is called superspin glass (SSG) [15], meaning superspin to be related to the total magnetic moment of a particle. Recently, the relaxation and memory effects in the magnetization of ferromagnetic nanoparticles have been in focus [16–19]. In general, the transition from the superparamagnetic (SPM) to the SSG state is pronounced in the temperature dependence of the magnetization of nanoparticle systems and determined by a set of certain critical indices, similar to the case of spin glasses [20].

We note that single-domain particles can be of the greatest interest because the single-domain threshold for nanoparticles will often be no larger than the correlation length of interacting spins in spin glass [21]. This allows one to consider each nanoparticle as a separate droplet. Many authors [19,22–25] demonstrated the possibility of tuning the magnetic interactions upon forming a coating of required thickness on the nanoparticle surface, which makes it possible to control the

*yuk@iph.krasn.ru

temperature of the transition to the SSG state. This fine tuning of the properties of ensembles of interacting nanoparticles can be used to implement the nonergodic magnetic systems with desired characteristics. In this paper, we explored the dynamics of the correlated magnetic moments depending on the existence of interparticle interactions by the example of ferrihydrite ($\text{Fe}_2\text{O}_3 \times n \cdot \text{H}_2\text{O}$) nanoparticles. The magnetic moments of iron atoms in ferrihydrite are ordered antiferromagnetically and the Néel temperature of the material is ~ 350 K [26]. Since ferrihydrite only exists on the nanoscale, its nanoparticles are a good model for studying the spin dynamics of the SSG state. As applied to antiferromagnetic nanoparticles, the superspin (the full magnetic moment of a particle) is an uncompensated moment caused by partial decompensation of the ferromagnetically ordered planes, which attains hundreds of Bohr magnetons for particles several nanometers in size [27–31]. To explore features of the spin dynamics in such systems, the dc and ac [$\chi'(T)$ and $\chi''(T)$] magnetic susceptibilities were measured in a weak magnetic field in the region of the SPM blocking for ensembles of interacting and noninteracting magnetic ferrihydrite nanoparticles. In addition, the behavior of the susceptibility was simulated at different frequencies of an ac magnetic field with allowance for the established size distribution of nanoparticles.

II. EXPERIMENTAL METHODS

The synthesis of a chemical sample (FH-chem) and the method for forming a controlled organic coating (FH-coated) on the nanoparticle surface were described in detail in Refs. [23,32]. The two samples under study were ensembles of ferrihydrite nanoparticles with fairly strong (sample FH-chem) and weak (sample FH-coated) magnetic interactions. Here, we only note that FH-chem is the synthetic ferrihydrite sample prepared by hydrolysis of iron (III) nitrate. Droplets of the 1M NaOH solution were added to the 100-ml $\text{Fe}(\text{NO}_3)_3 \cdot 9\text{H}_2\text{O}$ solution (0.2M) at a rate of 20 ml/min at room temperature under constant stirring until neutral pH. Then the precipitate was washed with de-ionized water to remove the remaining ions and dried at room temperature. The FH-coated sample was synthesized by arabinogalactan coating of the sample FH-chem, by additive of 1.0 g of arabinogalactan and sonication for 10 min (22 kHz, 50 W/cm²).

The microdiffraction and size distribution of the samples were studied by transmission electron microscopy (TEM). Specimens for the microscopy investigations were prepared by shaking the synthesized powder with alcohol in an ultrasonic bath and depositing the obtained suspension onto support meshes with perforated carbon. The TEM study was carried out on a Hitachi HT7700 transmission electron microscope at an accelerating voltage of 100 kV.

The microdiffraction analysis revealed two diffusion reflections corresponding to interplanar spacings of 1.5 and 2.6 Å for both samples. The average particle size was calculated using the Scherrer formula. A half width of the first brightest diffraction ring was taken into account when estimating the average particle diameter. According to the electron microdiffraction data, the average particle diameters were $\langle d \rangle \approx 2.7$ and 2.6 nm for samples FH-chem and FH-coated, respectively. In addition, the size distribution histograms were built using

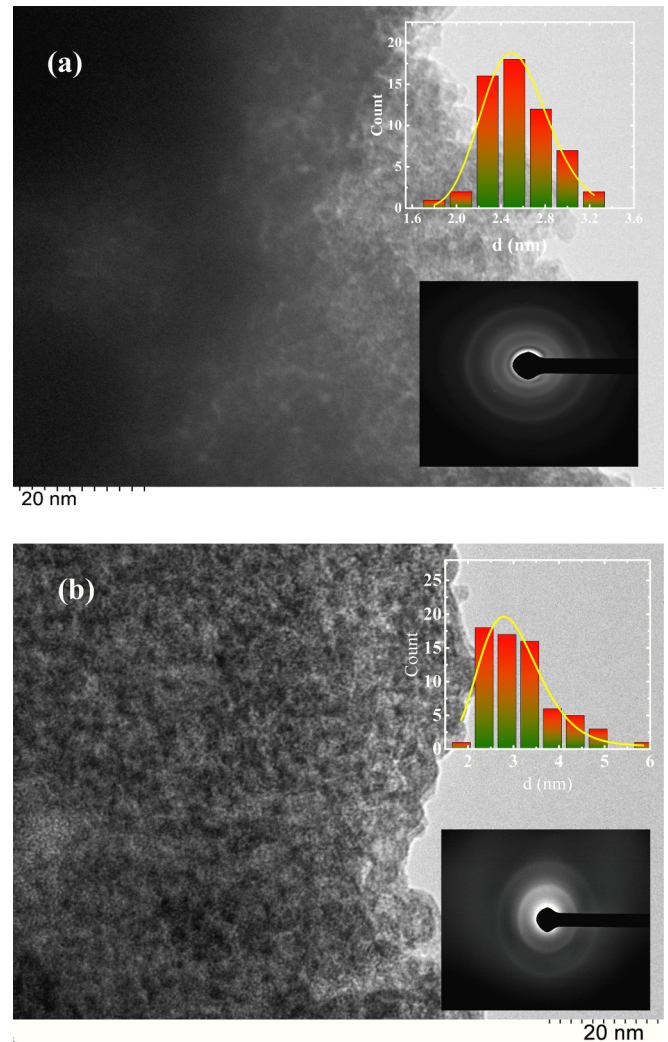


FIG. 1. TEM images of samples (a) FH-chem and (b) FH-coated. The upper insets show the calculated particle size; the solid line corresponds to the log-normal distribution law processing. The lower insets present microdiffraction patterns of the samples.

conventional computer tools (see the insets in Fig. 1). The average particle diameters found using the lognormal distribution approximation of the obtained histograms are $\langle d \rangle \approx 2.7$ and 3.0 nm for samples FH-chem and FH-coated, respectively, which is consistent with the Scherrer estimation.

The dc and ac magnetic properties of the samples were studied in a magnetic field of 2 Oe. The dc magnetization was measured with an original magnetometer [33]. The ac measurements of the dynamic susceptibilities $\chi'(T)$ and $\chi''(T)$ were performed on a Quantum Design physical property measurement system (PPMS-9) in a frequency range of 10–10 000 Hz.

III. RESULTS

Previously [23,32,34], we reported on the SPM behavior of ferrihydrite nanoparticles with and without coating. This is obviously due to the ultrafine nanoparticle size confirmed by the TEM study (Fig. 1). At such a particle size, the defect structure induces the uncompensated magnetic moment of a

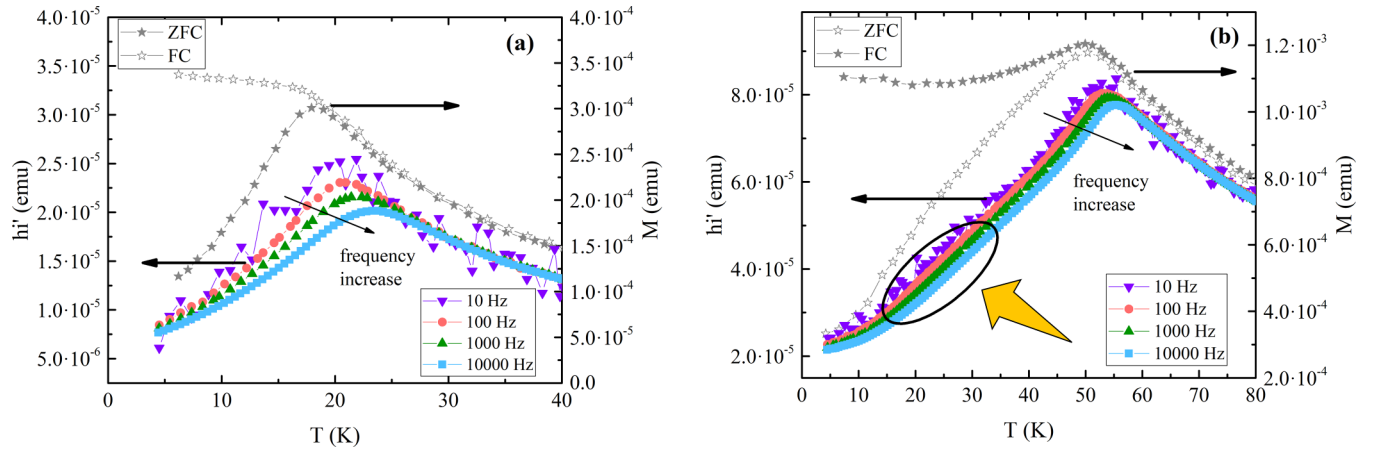


FIG. 2. Real part of the ac magnetic susceptibility of samples (a) FH-coated and (b) FH-chem. Temperature dependence of the field-cooled (FC) and zero-field-cooled (ZFC) static magnetization is also shown. The arrow and oval show the area of the susceptibility bending for sample FH-chem.

particle, which is blocked at a certain temperature called the SPM blocking temperature (T_B). The SPM blocking temperature for a system of noninteracting particles can be obtained from the Néel-Brown equation

$$T_B = \frac{K_{\text{eff}} V}{\ln(\tau_m / \tau_0) k_B}. \quad (1)$$

Here, K_{eff} is the effective magnetic anisotropy constant, which accounts for both the bulk and surface magnetic anisotropy; V is the particle volume; τ_m is the characteristic measuring time, which depends on the experimental technique used; and τ_0 is the characteristic relaxation time (in the unblocked state, τ_0 can lie within the interval of 10^{-9} – 10^{-13} s) [31]. In the measurements of the real part of the ac magnetic susceptibility or in the static magnetization measurements in sufficiently weak magnetic fields, the SPM blocking temperature can be determined as a maximum point in the $\chi'(T)$ or $M(T)$ dependence obtained under the zero-field-cooling (ZFC) conditions.

In Fig. 2, the static $M(T)$ data obtained in the ZFC measurement protocol are presented together with the real $\chi'(T)$ data. It can be seen that, for both samples, the $\chi'(T)$ behavior above the maximum point is independent of the frequency of the applied field and tends to the $M(T)$, thereby indicating the equilibrium state of the magnetic system, which is no longer reached below the blocking temperature. In addition, one can see the shift of the peak position with the increasing measuring frequency, which is related to a decrease in the characteristic measuring time: According to Eq. (1), $\tau_m = 1/\omega$, where ω is the cyclic frequency of an ac magnetic field. The numerical values of the blocking temperatures for the dc susceptibility are 19.0 and 50.4 K for samples FH-coated and FH-chem, respectively (Fig. 2).

The blocking temperature of the sample with interacting particles (FH-chem) is significantly higher than that of sample FH-coated. As we showed previously [32,35], the static magnetization of sample FH-chem exhibits features of strong interparticle interactions [the $M(T)$ FC dependence below the blocking temperature is nonmonotonic]. Instead of Eq. (1), the SPM blocking behavior should be described by the Vogel-Fulcher dependence, which takes into account

the interparticle interactions as a shift of T_B toward higher temperatures [31,36],

$$T_B - T_0 = \frac{K_{\text{eff}} V}{\ln(\tau_m / \tau_0) k_B}. \quad (2)$$

Here, parameter T_0 determines the degree of interparticle interactions, which are noticeably stronger at T_0 than at T_B [37–40]. In addition to the above-mentioned T_B shift, the interparticle interactions cause the formation of the spin-glass-like state, which has been observed in various systems of magnetic nanoparticles [10,41–45]. The organic coating of nanoparticles leads, at first glance, to the complete disappearance of this state; however, as was mentioned above, there are signs of the absence of thermodynamic equilibrium in the system below T_B for both samples.

The greatest differences are observed between the temperature dependences of the imaginary (out-of-phase) susceptibility of the two samples (Fig. 3). The contribution of the interparticle interactions manifests itself in the growth of the imaginary susceptibility signal $\chi''(T)$ with increasing frequency for sample FH-chem, while sample FH-coated with weakly interacting particles yields the opposite picture. For sample FH-coated, one can see a single broad maximum, while in the case of FH-chem, a secondary local $\chi''(T)$ extremum is pronounced. The main peak with the higher intensity for sample FH-chem corresponds to the temperature of blocking of the nanoparticle magnetic moments obtained from the $\chi'(T)$ data, whereas the local maximum on a “shoulder” results from the complex process of relaxation of the magnetic moments of strongly interacting nanoparticles in this sample [42–46]. The observed local $\chi''(T)$ maximum has a much smaller value, which depends strongly on frequency. Thus, the freezing of the magnetic moments triggers a complex mechanism of the magnetic energy dissipation in sample FH-chem, which consists of at least two stages corresponding apparently to two independent magnetic processes. A similar behavior was reported for core-shell Fe/ γ -Fe₂O₃ particles in Refs. [10,41], where the dissipative process was explained by the independent freezing of the core and shell spins, which is indicative of decoupling of the core and shell magnetic

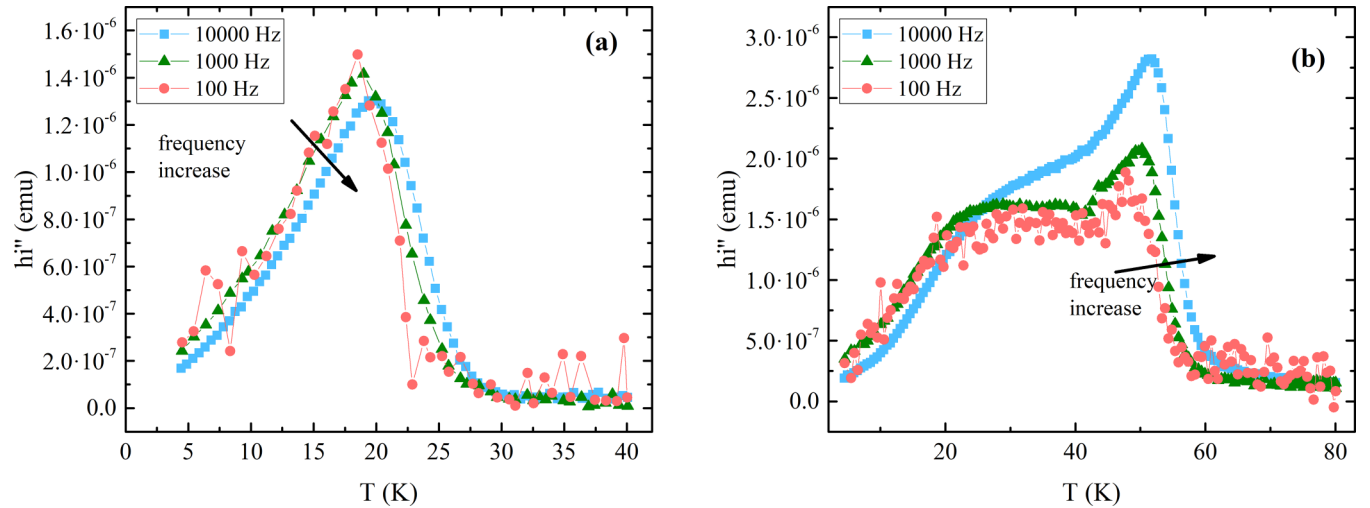


FIG. 3. Imaginary part of the ac magnetic susceptibility of samples (a) FH-coated and (b) FH-chem. The arrow shows the frequency growth direction.

systems in particles at certain frequencies of the magnetic field. The additional shoulder in the temperature dependence of the imaginary part of the susceptibility is characteristic also of spin-glass bulk materials [4,47,48], which evidences for its general origin.

IV. DISCUSSION

The analysis of the low-temperature behavior of the $\chi'(T)$ dependence for sample FH-chem revealed an inflection in the curve (oval in Fig. 2). The temperature range of this singularity is consistent with the temperature range of the shoulder in the out-of-phase susceptibility (Fig. 3). At the same time, the sample with the weak interactions between particles (FH-coated) does not exhibit such a behavior and yields no local $\chi''(T)$ maximum. Hence, the additional shoulder in the $\chi''(T)$ dependence can be interpreted as a manifestation of the collective effect of freezing of the magnetic moments (spins of iron atoms) on the nanoparticle surface. Taking into account the strong interparticle interactions in sample FH-chem, it is reasonable to assume that the observed freezing of the surface spins is related precisely to the interparticle interactions.

A similar behavior was reported in Ref. [42], where the effect of aging of ferrihydrite nanoparticles on the shape of the $\chi'(T)$ and $\chi''(T)$ dependences was explored. Strongly interacting nanoparticles yielded a secondary susceptibility maximum, which disappeared as nanoparticles grew in size and transformed into hematite. The magnetic interactions between nanoparticles can be implemented through the dipole-dipole interactions of the particle's own spins (super-spins) or through the indirect exchange coupling between the atomic magnetic moments mediated by the matrix material, which slows down the spin dynamics (see the last column in Table I) as compared with the case of a canonical spin glass, for which this time is close to the microscopic atomic spin flip time ($\sim 10^{-13}$ s) [49]. The dipole interaction energy for two interacting nanoparticles is no higher than ~ 1 K [42,50,51]; therefore, the observed addition to the blocking temperature cannot be made by only the dipole interactions. Obviously, the

main contribution is provided by the exchange coupling. The exchange coupling can easily occur in the uncoated sample (FH-chem), taking into account the low ζ potential of ferrihydrite nanoparticles, which manifests itself in their strong aggregation [52]. Thus, ferrihydrite nanoparticles can form strongly coupled clusters, which is reflected in a fairly high blocking temperature of sample FH-chem, in contrast to the sample of coated nanoparticles. In the latter, the coating weakens the aggregation of nanoparticles, which obviously affects the cluster size and, consequently, lowers the interparticle interaction energy, although, as we show below, the complete destruction of nanoparticle clusters does not occur.

As was established empirically, the frequency shift of the maximum temperature T_B in the $\chi'(T)$ dependence is determined by Eq. (3) and represents a good criterion for distinguishing reliably the spin-glass states from the SPM behavior of nanoparticles [53]:

$$\Gamma = \frac{\Delta T_B}{T_B \Delta(\log \omega)}. \quad (3)$$

Here, ΔT_B is the frequency shift of the susceptibility peak, T_B is the maximum temperature of the real part of the susceptibility, and ω is the cyclic frequency of the ac magnetic field. This characteristic provides quantitative information about the degree of collective effects in the magnetic behavior of nanoparticles. The Γ values for the samples under study are given in Table I. As was mentioned in Ref. [15], this parameter for the SPM ensembles is $\Gamma > 0.10$, while for canonical spin glasses it is much lower: $\Gamma \approx 0.002\text{--}0.004$. The intermediate values ($\Gamma < 0.06$) are characteristic of SSG or cluster spin glasses [10,46,54]. Thus, the formation of a spin-glass magnetic structure in a nanoparticle ensemble below T_B is a manifestation of the interparticle magnetic interactions, which lead to the occurrence of a cluster of interacting nanoparticles, similar to that described within the Fisher droplet model [9].

The Γ values obtained for the two samples are no higher than 0.06, which is indicative of the effect of interparticle interactions in them [10,15,41]; however, a three times higher Γ value for nanoparticles with the organic coating shows that

TABLE I. Data analysis of the relaxation dynamics in the two samples of ferrihydrite nanoparticles ensembles on the basis of the power-law spin dynamics.

Sample	Γ (arb. units)	T_g (K)	$z\nu$ (arb. units)	E_{int} [23]	τ_0 (s)
FH-chem	0.019	49.5	5.9	121	2.0×10^{-12}
FH-coated	0.057	18	8.0	27	1.0×10^{-12}

sample FH-coated approaches an ensemble of noninteracting particles [55]. Recently [23], we observed a partial effect of the interparticle interactions in sample FH-coated when studying the SPM relaxation in detail by Mössbauer spectroscopy. The organic coating naturally reduces the size of a cluster of interacting nanoparticles, which causes a change in the spin dynamics. As shown in Ref. [46], this change is related primarily to the magnetic moments on the surface of nanoparticles inside a cluster. According to the droplet model [9], the magnetic correlation length ξ is the length scale above which the field destroys the equilibrium state of a zero-field spin glass. In the case of nanoparticles, this parameter is physically limited by the size of a cluster of aggregated particles, which governs the behavior of the entire system.

The measured ac susceptibility values, together with the Mössbauer data obtained previously, allowed us to get a complete picture of the relaxation behavior of the nanoparticle magnetic moments presented in Fig. 4, which shows the data on the temperature maxima of the dependence of $\chi'(T)$ on relaxation time τ ($\tau = 1/\omega$) obtained by different techniques. The frequency dependence of the freezing temperature T_g in the scaling theories of spin glasses is modeled by a power-law functional dependence, which predicts a critical slowdown of the spin dynamics and divergence of the $\tau(T)$ dependence during the spin-glass transition:

$$\tau = \tau_0 \left(\frac{T}{T_g} - 1 \right)^{-z\nu}. \quad (4)$$

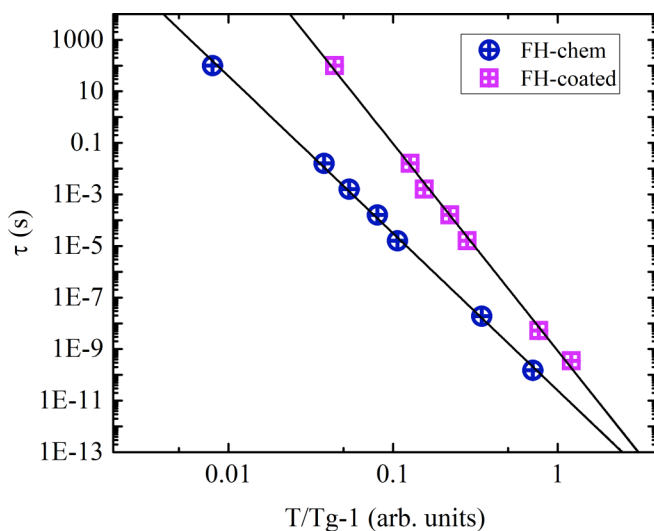


FIG. 4. Critical slowing down of the time of SPM relaxation of the magnetic moment in samples FH-coated and FH-chem obtained by Mössbauer spectroscopy and ac and dc magnetization measurements. Straight solid lines show the result of fitting by Eq. (4).

Here, ν is the critical exponent of correlation length ξ and z is the dynamic index: $\tau \sim \xi^z$ [54]. The numerical result of the processing is given in Table I and Fig. 4 shows the temperature dependence of the relaxation time with allowance for our results from Refs. [23,35]. The figure presents the extended picture of the relaxation dynamics of the magnetic moments, compared to previous papers [10,41], and its change under the action of the interparticle interactions (time τ from 10^{-10} to 100 s). The linearization of these sets of points in double logarithmic coordinates allows us to obtain the critical indices for both samples. The obtained values are common for nanoparticles' systems [10,41,46]. It should be mentioned that the range of $z\nu$ is quite wide. Nevertheless, we may argue that coating process leads to the rise of $z\nu$ parameter. Figure 4 demonstrates the evident slope change, which indicates a more rapid relaxation rate in FH-coated compared with the FH-chem sample. It may be understood as a lowering of the effective volume of the magnetic clusters in the FH-coated with the decrease of the contribution of interactions and, consequently, the faster relaxation rate.

In Ref. [56], it was noted that an isotropic Heisenberg spin glass is characterized by a value of $z\nu \sim 6-8$, while this parameter for an Ising-type spin glass is $z\nu \sim 10-12$. Therefore, taking into account the results obtained, we can say that the ferrihydrite samples behave similarly to the Heisenberg spin glass, which is natural for nanoparticle ensembles. There exist nanoparticle ensembles with the critical indices similar to that of ferrihydrite [10,41,46,57]. Thus, with a decrease in the interparticle interaction energy, the critical index $z\nu$ grows. (Meanwhile, as reported in Refs. [13,43], some materials can exhibit the Ising-type spin-glass behavior at fairly small $z\nu$ values.)

The partial preservation of the interactions after coating ensures the validity of the scaling dependence for sample FH-coated. Generally, we can state that the interactions give rise to the spin-glass-like behavior of the samples. Based on the current data and on the series of previously published papers [10,41,43,46], we may argue a strong interparticle interactions is a primary cause for the spin-glass-like state formation in ferrihydrite ensembles.

Besides, such a behavior takes place in the appropriate form of the temperature dependence of the out-of-phase susceptibility. Usually, the most attention is paid to the real part of the magnetic susceptibility (χ'), when analyzing data on ac-magnetic susceptibility behavior, and, commonly, only the position of the maximum of the dependence $\chi'(T)$ is used to show the frequency shift. Such an analysis was carried out in the first part of this section. As for the out-of-phase magnetic susceptibility, it is admittedly that it describes the energy dissipation for any system, including the magnetic nanoparticle systems. The energy dissipation process is closely related to the applied features of magnetic nanoparticles, for

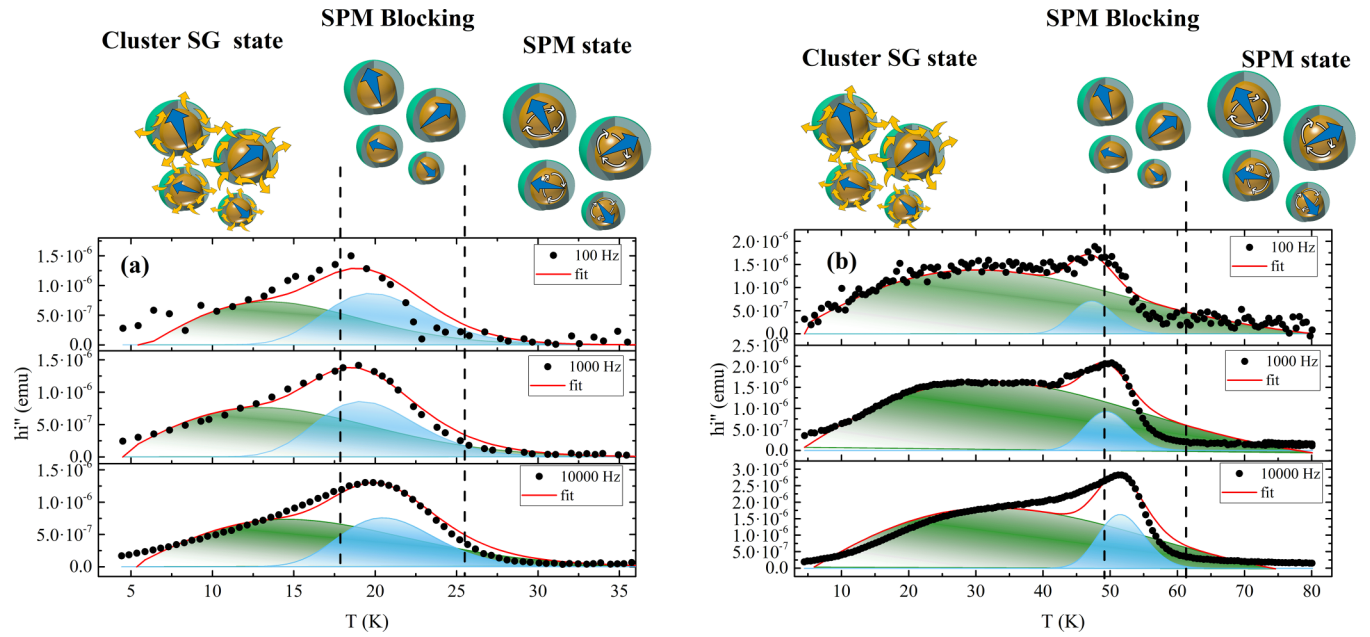


FIG. 5. Simulated $\chi''(T)$ dependences of samples (a) FH-coated and (b) FH-chem (solid line). The shaded areas refer to the two magnetic subsystems in the samples. At the top: scheme of the magnetic states.

example, the specific absorption rate (SAR), which is the power released by the particles in the form of heat in magnetic hyperthermia [58,59]. Therefore, we suggest to pay more attention to the analysis of the out-of-phase magnetic susceptibility.

The analysis of the temperature dependences of the ac magnetization can yield the quantitative magnetic characteristics of nanoparticle ensembles. The Monte Carlo simulation of the magnetic behavior of ultrafine (~ 2 nm) MnFe_2O_4 nanoparticles with regard to both the intra- and interparticle interactions showed good agreement with the experimental static magnetization data [60]. In Refs. [14,61], the possibility of modeling of the imaginary part (out of phase) of the ac susceptibility with allowance for the magnetic field frequency was demonstrated for magnetic nanoparticles with a certain size distribution and interparticle interactions. Taking these results into account, here we processed the experimental data presented in Fig. 3. Since we have

$$\chi'' = c \cdot \psi(f, \gamma) \frac{\theta^*}{\theta_0^2} \exp\left(-\frac{\ln^2(\theta^*/\theta_0^2)}{2\delta_\theta^2}\right), \quad (5)$$

where $\theta^* = \sigma^* T = -T \ln(2\pi f \tau_0)$, $c = \sqrt{\frac{\pi}{2}} N \frac{(M_s V_0)^2}{6k_B \delta_\theta}$, $\theta_0 = \frac{E_A}{k_B}$, and $\psi(f, \gamma)$ is the function determined by Landi *et al.* [59,61] by the mean-field approximation and taking into account interparticle interactions, M is the particle magnetic moment taken to be $170\mu_B$, [34], and δ is the width of the particle size distribution, which was used as a fitting parameter. The anisotropy energy $E_A = K_{\text{eff}}V$ was used as E_A for nanoparticles.

Since the experimental dependences contain local maxima, along with the true extremum (see Fig. 3), the computer fitting

was performed for the function

$$\psi(f, \gamma) \cdot \sum_{i=1}^{n_K} q_i \frac{\theta^*}{\theta_{0,i}^2} \exp\left(-\frac{\ln^2(\theta^*/\theta_{0,i}^2)}{2\delta_\theta^2}\right). \quad (6)$$

Here, n_K is generally the number of magnetic subsystems (in our fitting, $n_K = 2$) and q_i is their weight factor, which was varied during the simulation. In our case, the fitting was performed for two independent magnetic subsystems. The result of fitting of the $\chi''(T)$ dependences for the two samples is shown in Fig. 5 and the numerical results are given in Table II.

Fitting of the $\chi''(T)$ dependences for both samples showed that they contain at least two independent components. The mathematical processing of the right-hand side of the $\chi''(T)$ dependences [the pronounced $\chi''(T)$ maximum] agrees with a fairly narrow distribution of nanoparticles with an average diameter of 2.7 nm in an ensemble for both samples, which is consistent with the TEM data. The widths of the obtained distributions also correlate with the electron microscopy data. Therefore, this component is responsible for blocking of the particle magnetic moment. The left-hand side has a much wider distribution, which is not reflected in the TEM data and, consequently, cannot be a manifestation of blocking of the magnetic moments of nanoparticles themselves, but refers to the energy dissipation via the formation of a spin-glass structure. The integral fractions of the discussed components for samples FH-chem and FH-coated are drastically different (see the last column in Table II). In sample FH-chem with strong interparticle interactions, the energy dissipation occurs mainly by means of the shell component [the left-hand side of the $\chi''(T)$ dependence], while in sample FH-coated the shell subsystem is manifested much weaker. The frequency

TABLE II. Results of the mathematical modeling of the out-of-phase ac susceptibility of samples FH-chem and FH-coated. E_p is the magnetic energy of nanoparticles, E_{SG} is the energy of freezing of the magnetic moments, and δ_{core} and δ_s are the core and shell distribution widths, respectively. The ratio between areas under the curves is given in the last column.

Sample	f (Hz)	E_p ($\times 10^{-15}$ ergs)	E_{SG} ($\times 10^{-15}$ ergs)	δ_{core}	δ_s	Core/shell fraction
FH-chem	100	4.5 ± 0.4	2.5 ± 0.4	0.07	1.3	0.10 ± 0.02
FH-coated	100	3.1 ± 0.3	1.1 ± 0.2	0.16	1.2	0.66 ± 0.02
FH-chem	1000	4.5 ± 0.4	2.5 ± 0.4	0.07	1.1	0.14 ± 0.02
FH-coated	1000	3.1 ± 0.3	1.1 ± 0.2	0.16	0.95	0.67 ± 0.02
FH-chem	10000	4.5 ± 0.4	2.5 ± 0.4	0.07	1.1	0.21 ± 0.02
FH-coated	10000	3.1 ± 0.3	1.1 ± 0.2	0.16	0.95	0.65 ± 0.02

dependences of these fractions are also fundamentally different. In sample FH-chem, the core/shell area ratio depends significantly on the field frequency. This is probably due to the aforementioned decoupling of the core and shell magnetic systems inside particles under the action of the interparticle interactions [46]. This is confirmed by the almost complete absence of a frequency dependence of the core and shell fractions in the dissipative process for sample FH-coated.

At first sight, the above-described behavior seems unrealistic for a single-phase system. However, as was shown previously, the ferrihydrite surface structure is strongly depleted in iron and enriched in OH groups and differs significantly from the structure of the particle core [62,63], which was confirmed by the low fractal dimensionality of ferrihydrite [64,65]. Such rarefaction of the nanoparticle surface with increasing distance from the core leads to the formation of a denser crystalline core and a rarefied shell [34]. This explains well the observed core-shell magnetic structure.

The second column in Table II gives the fitting values of the nanoparticle magnetic energy E_p . This energy takes into account the energy of the magnetic anisotropy (volume and surface) of ferrihydrite nanoparticles in the two samples. In the $\chi''(T)$ simulation, the energy of the strong interparticle interactions characteristic of sample FH-chem was taken into account separately from E_p in the $\psi(f, \gamma)$ function, according to the formulas from Ref. [59], and corresponded to the temperature shift of the susceptibility maximum [T_0 in Eq. (2)]. In our case, the T_0 values for samples FH-chem and FH-coated were 24 and 7 K, respectively. Using the obtained E_p values, we found the magnetic anisotropy constants K_{eff} to be $23 \pm 2 \times 10^5$ and $17 \pm 2 \times 10^5$ ergs/cm³ for samples FH-chem and FH-coated, respectively. These values are in good agreement with a value of 21×10^5 ergs/cm³ obtained previously in Ref. [35], which confirms the applicability of the approach used to simulate the $\chi''(T)$ dependences. It should be noted, however, that the shift of the maximum susceptibility at the temperature T_0 (manifestation of the interparticle interactions) and the magnetic energy dissipation during freezing of the magnetic moments on the particle surface (parameter E_{SG} , second column in Table II) not only refer to two different processes, but appear to be mutually independent. On the other hand, the freezing of the magnetic moments on the nanoparticle surface is a direct consequence of the interparticle interactions. Therefore, it can be assumed that the left-hand side of the curves of the out-of-phase ac susceptibility (the wide green distribution in Fig. 5) corresponds to the

energy loss caused by the interparticle magnetic interactions inside nanoparticle clusters, which form the spin-glass-like state already below the blocking temperature. This process is most pronounced in sample FH-chem and almost completely reduced in sample FH-coated. In addition, it is noteworthy that this effectively manifests itself in interacting ferrihydrite nanoparticles, similar to the case of core-shell nanoparticles.

It is known well that the magnetic moment of each ion in a spin glass below the freezing temperature is localized mainly along the local easy magnetization axis determined by a local crystal field. This is equivalent to a random change in the crystal field under frustrations of the exchange coupling or a strong dilution of magnetic ions in a bulk material. This is how a noncollinear spin-glass structure is formed [9,53]. In nanoscale systems, a similar effect is induced by a random distribution of the anisotropy axes of separate but interacting nanoparticles. Under the interparticle interactions, a certain correlated structure of spins forms on the surface of different particles

V. CONCLUSIONS

To sum up, we note that the unique morphology of nanoparticles of ferrihydrite, which, on the one hand, is hydrated iron oxide and, on the other hand, has a dense well-crystallized core, gives rise to the intriguing phenomenon of splitting of the nanoparticle magnetic structure into two independent subsystems. It was shown by measuring the ac magnetic susceptibility that the magnetic behavior of the ensembles of ferrihydrite nanoparticles repeats largely the observed behavior of core-shell systems [10,41]. This was attributed to the interparticle magnetic interactions, which determine, to a great extent, the shape of the $\chi''(T)$ dependences below the blocking temperature and form a spin-glass-like structure. The organic coating of ferrihydrite particles weakens significantly the energy of the interparticle interactions (obviously, due to a decrease in the nanoparticle cluster size); therefore, the spin-glass state does not form. At the same time, a decrease in the density of nanoparticles themselves from the core to the periphery is preserved [34], which is reflected in an additional broad component of the energy dissipation in the $\chi''(T)$ simulation and the increasing parameter Γ of the frequency shift of the magnetic susceptibility peak for sample FH-coated. The calculated values of this parameter ($\Gamma < 0.06$) appeared to be similar to the Γ values for the SSG or cluster-type spin-glass state. It was established using

the processing of the temperature dependence of the relaxation time for the ferrihydrite nanoparticle ensembles by the scaling law that the obtained critical indices $z\nu$ are characteristic of this magnetic state. It was found that the coating of nanoparticles increases this parameter from $z\nu = 5.9$ for sample FH-chem to $z\nu = 8.0$ for sample FH-coated. Thus, via increasing the nanoparticle blocking temperature, the surface modification by an organic coating affects noticeably the spin dynamics of the investigated nanoparticle ensembles below the temperature of blocking of the magnetic moments.

ACKNOWLEDGMENTS

The electron microscopy study and ac susceptibility measurements were carried out on the equipment of the Krasnoyarsk Territorial Center for Collective Use, Krasnoyarsk Scientific Center, Siberian Branch of the Russian Academy of Sciences. This study was supported by the Russian Science Foundation, Project No. 21-72-00025 Tuning the Magnetic Properties of Ultrafine Biocompatible Ferrihydrite Nanoparticles through Interparticle Interactions [66].

- [1] J. Mydosh, *Europhys. News* **14**, 2 (1983).
- [2] J. Mydosh, *Hyperfine Interact.* **31**, 347 (1986).
- [3] A. Cabot, F. Carollo, and I. Lesanovsky, *Phys. Rev. B* **106**, 134311 (2022).
- [4] G. F. Goya and V. Sagredo, *Phys. Rev. B* **64**, 235208 (2001).
- [5] F. F. Barquín, J. Sal, P. Gorria, J. Garitaonandia, and J. Barandiarán, *Eur. Phys. J. B* **35**, 3 (2003).
- [6] J. F. Ding, O. I. Lebedev, S. Turner, Y. F. Tian, W. J. Hu, J. W. Seo, C. Panagopoulos, W. Prellier, G. Van Tendeloo, and T. Wu, *Phys. Rev. B* **87**, 054428 (2013).
- [7] I. Lyubutin, N. Y. Korotkov, K. Frolov, N. Kazak, M. Platunov, Y. V. Knyazev, L. Bezmaternykh, S. Ovchinnikov, A. Arauzo, and J. Bartolomé, *J. Alloys Compd.* **642**, 204 (2015).
- [8] M. Weissman, *Rev. Mod. Phys.* **65**, 829 (1993).
- [9] D. S. Fisher and D. A. Huse, *Phys. Rev. B* **38**, 386 (1988).
- [10] S. Chandra, H. Khurshid, W. Li, G. C. Hadjipanayis, M. H. Phan, and H. Srikanth, *Phys. Rev. B* **86**, 014426 (2012).
- [11] Q. Zhai, V. Martin-Mayor, D. L. Schlagel, G. G. Kenning, and R. L. Orbach, *Phys. Rev. B* **100**, 094202 (2019).
- [12] Q. Zhai, I. Paga, M. Baity-Jesi, E. Calore, A. Cruz, L. A. Fernandez, J. M. Gil-Narvion, I. Gonzalez-Adalid Pearnin, A. Gordillo-Guerrero, D. Iñiguez, A. Maiorano, E. Marinari, V. Martin-Mayor, J. Moreno-Gordo, A. Muñoz-Siduepe, D. Navarro, R. L. Orbach, G. Parisi, S. Perez-Gaviro, F. Ricci-Tersenghi, J. J. Ruiz-Lorenzo, S. F. Schifano, D. L. Schlagel, B. Seoane, A. Tarancon, R. Tripicciono, and D. Yllanes, *Phys. Rev. Lett.* **125**, 237202 (2020).
- [13] C. Djurberg, P. Svedlindh, P. Nordblad, M. F. Hansen, F. Bødker, and S. Mørup, *Phys. Rev. Lett.* **79**, 5154 (1997).
- [14] D. E. Madsen, M. F. Hansen, and S. Mørup, *J. Phys.: Condens. Matter* **20**, 345209 (2008).
- [15] J. Dormann, L. Bessais, and D. Fiorani, *J. Phys. C* **21**, 2015 (1988).
- [16] S. Mørup, M. B. Madsen, J. Franck, J. Villadsen, and C. J. Koch, *J. Magn. Magn. Mater.* **40**, 163 (1983).
- [17] R. K. Zheng, H. Gu, B. Xu, and X. X. Zhang, *Phys. Rev. B* **72**, 014416 (2005).
- [18] M. Sasaki, P. E. Jönsson, H. Takayama, and H. Mamiya, *Phys. Rev. B* **71**, 104405 (2005).
- [19] R. Cohen, G. Cody, M. Coutts, and B. Abeles, *Phys. Rev. B* **8**, 3689 (1973).
- [20] M. S. Andersson, R. Mathieu, P. S. Normile, S. S. Lee, G. Singh, P. Nordblad, and J. A. De Toro, *Mater. Res. Express* **3**, 045015 (2016).
- [21] A. Mathur, P. Loskill, K. Shao, N. Huebsch, S. Hong, S. G. Marcus, N. Marks, M. Mandegar, B. R. Conklin, L. P. Lee *et al.*, *Sci. Rep.* **5**, 8883 (2015).
- [22] T. S. Berquó, J. J. Erbs, A. Lindquist, R. L. Penn, and S. K. Banerjee, *J. Phys.: Condens. Matter* **21**, 176005 (2009).
- [23] Y. V. Knyazev, D. A. Balaev, R. N. Yaroslavtsev, A. A. Krasikov, D. A. Velikanov, Y. L. Mikhlin, M. N. Volochaev, O. A. Bayukov, S. V. Stolyar, and R. S. Iskhakov, *Adv. Nano Res.* **12**, 605 (2022).
- [24] P. R. Rojas, P. Tancredi, O. M. Londoño, M. Knobel, and L. M. Socolovsky, *J. Magn. Magn. Mater.* **451**, 688 (2018).
- [25] W. C. Nunes, L. M. Socolovsky, J. C. Denardin, F. Cebollada, A. L. Brandl, and M. Knobel, *Phys. Rev. B* **72**, 212413 (2005).
- [26] M. S. Seehra, V. S. Babu, A. Manivannan, and J. W. Lynn, *Phys. Rev. B* **61**, 3513 (2000).
- [27] S. Popkov, A. Krasikov, D. Velikanov, V. Kirillov, O. Martyanov, and D. Balaev, *J. Magn. Magn. Mater.* **483**, 21 (2019).
- [28] S. Popkov, A. Krasikov, A. Dubrovskiy, M. Volochaev, V. Kirillov, O. Martyanov, and D. Balaev, *J. Appl. Phys.* **126**, 103904 (2019).
- [29] T. Iimori, Y. Imamoto, N. Uchida, Y. Kikuchi, K. Honda, T. Iwahashi, and Y. Ouchi, *J. Appl. Phys.* **127**, 023902 (2020).
- [30] D. Balaev, A. Krasikov, S. Popkov, S. Semenov, M. Volochaev, D. Velikanov, V. Kirillov, and O. Martyanov, *J. Magn. Magn. Mater.* **539**, 168343 (2021).
- [31] S. Mørup, D. E. Madsen, C. Frandsen, C. R. Bahl, and M. F. Hansen, *J. Phys.: Condens. Matter* **19**, 213202 (2007).
- [32] Y. V. Knyazev, D. Balaev, S. Stolyar, A. Krasikov, O. Bayukov, M. Volochaev, R. Yaroslavtsev, V. Ladygina, D. Velikanov, and R. Iskhakov, *J. Alloys Compd.* **889**, 161623 (2021).
- [33] D. A. Velikanov, *Sib. J. Sci. Technol.* **2**, 176 (2013).
- [34] Y. V. Knyazev, D. Balaev, S. Stolyar, O. Bayukov, R. Yaroslavtsev, V. Ladygina, D. Velikanov, and R. Iskhakov, *J. Alloys Compd.* **851**, 156753 (2021).
- [35] D. Balaev, S. Stolyar, Y. V. Knyazev, R. Yaroslavtsev, A. Pankrats, A. Vorotynov, A. Krasikov, D. Velikanov, O. Bayukov, V. Ladygina *et al.*, *Results Phys.* **35**, 105340 (2022).
- [36] D. Balaev, S. Semenov, A. Dubrovskiy, S. Yakushkin, V. Kirillov, and O. Martyanov, *J. Magn. Magn. Mater.* **440**, 199 (2017).
- [37] O. Petracic, X. Chen, S. Bedanta, W. Kleemann, S. Sahoo, S. Cardoso, and P. Freitas, *J. Magn. Magn. Mater.* **300**, 192 (2006).

- [38] C. Vieira, R. C. Gomes, F. Silva, A. Dias, R. Aquino, A. Campos, and J. Depeyrot, *J. Phys.: Condens. Matter* **31**, 175801 (2019).
- [39] J. Mohapatra, A. Mitra, D. Bahadur, and M. Aslam, *J. Alloys Compd.* **628**, 416 (2015).
- [40] A. M. Pereira, C. Pereira, A. S. Silva, D. S. Schmool, C. Freire, J.-M. Greneche, and J. P. Araujo, *J. Appl. Phys.* **109**, 114319 (2011).
- [41] Z. Nematı, H. Khurshid, J. Alonso, M. Phan, P. Mukherjee, and H. Srikanth, *Nanotechnology* **26**, 405705 (2015).
- [42] L. Gutiérrez, V. Barrón, M. Andrés-Vergés, C. Serna, S. Veintemillas-Verdaguer, M. Morales, and F. Lázaro, *J. Geophys. Res.: Solid Earth* **121**, 4118 (2016).
- [43] J. De Toro, S. Lee, D. Salazar, J. Cheong, P. Normile, P. Muniz, J. Riveiro, M. Hillenkamp, F. Tournus, A. Tamion *et al.*, *Appl. Phys. Lett.* **102**, 183104 (2013).
- [44] M. Gruyters, *Phys. Rev. Lett.* **95**, 077204 (2005).
- [45] D. Peddis, C. Cannas, G. Piccaluga, E. Agostinelli, and D. Fiorani, *Nanotechnology* **21**, 125705 (2010).
- [46] E. M. Jefremovas, J. Alonso, M. De la Fuente Rodríguez, J. Rodríguez Fernández, J. Espeso, D. Rojas, A. García-Prieto, M. Fernández-Gubieda, and L. Fernández Barquín, *Nanomaterials* **10**, 1117 (2020).
- [47] V. Dupuis, E. Vincent, J.-P. Bouchaud, J. Hammann, A. Ito, and H. A. Katori, *Phys. Rev. B* **64**, 174204 (2001).
- [48] M. Viswanathan and P. S. Anil Kumar, *Phys. Rev. B* **80**, 012410 (2009).
- [49] R. Mathieu, D. Akahoshi, A. Asamitsu, Y. Tomioka, and Y. Tokura, *Phys. Rev. Lett.* **93**, 227202 (2004).
- [50] S. Mørup, *Europhys. Lett.* **28**, 671 (1994).
- [51] B. Vanderstraeten, P. W. Chin, M. Fix, A. Leal, G. Mora, N. Reynaert, J. Seco, M. Soukup, E. Spezi, W. De Neve *et al.*, *Phys. Med. Biol.* **52**, 539 (2007).
- [52] J. Liu, S. M. Louie, C. Pham, C. Dai, D. Liang, and Y. Hu, *Environ. Res.* **172**, 552 (2019).
- [53] J. A. Mydosh, *Spin Glasses: An Experimental Introduction* (CRC Press, Boca Raton, FL, 1993).
- [54] A. Kumar, A. Senyshyn, and D. Pandey, *Phys. Rev. B* **99**, 214425 (2019).
- [55] M. Tadic, D. Nikolic, M. Panjan, and G. R. Blake, *J. Alloys Compd.* **647**, 1061 (2015).
- [56] R. Mathieu, A. Asamitsu, Y. Kaneko, J. P. He, and Y. Tokura, *Phys. Rev. B* **72**, 014436 (2005).
- [57] S. Nayak, S. Ghorai, A. M. Padhan, S. Hajra, P. Svedlindh, and P. Murugavel, *Phys. Rev. B* **106**, 174402 (2022).
- [58] J.-L. Déjardin, F. Vernay, and H. Kachkachi, *J. Appl. Phys.* **128**, 143901 (2020).
- [59] G. T. Landi, *Phys. Rev. B* **89**, 014403 (2014).
- [60] M. Vasilakaki, G. Margaris, D. Peddis, R. Mathieu, N. Yaacoub, D. Fiorani, and K. Trohidou, *Phys. Rev. B* **97**, 094413 (2018).
- [61] G. T. Landi, F. R. Arantes, D. R. Cornejo, A. F. Bakuzis, I. Andreu, and E. Natividad, *J. Magn. Magn. Mater.* **421**, 138 (2017).
- [62] T. Hiemstra, *Geochim. Cosmochim. Acta* **105**, 316 (2013).
- [63] T. Hiemstra, *Geochim. Cosmochim. Acta* **158**, 179 (2015).
- [64] P. Weidler and H. Stanjek, *Clay Miner.* **33**, 277 (1998).
- [65] B. A. Legg, M. Zhu, L. R. Comolli, B. Gilbert, and J. F. Banfield, *Langmuir* **30**, 9931 (2014).
- [66] <https://rscf.ru/project/21-72-00025/>.